PAPER

Check for updates

A polypropylene mesh coated with interpenetrating double network hydrogel for local drug delivery in temporary closure of open abdomen†

Ze Li,[a] Changliang Wu,[a] Zhen Liu,[a] Zhenlu Li,[a] Xingang Peng,[a] Jinjian Huang,*[ab] Jianan Ren [iD] *[ab] and Peige Wang*[a]

Prosthetic materials are widely used for temporary abdominal closure after open abdomen (OA), but local adhesion, erosion and fistula formation caused by current materials seriously affect the quality of life of patients. Recently, a three-dimensional porous network structure hydrogel has been used to simulate cell extracellular matrix that can support cell growth and tissue regeneration. In this study, we prepared an interpenetrating double-network hydrogel by photoinitiating glycidyl methacrylate-conjugated xanthan (XG) and 4-arm polyethylene glycol thiol (TPEG). This double-network hydrogel combined stiffness and deformation ability as well as *in situ* forming property, which could coat polypropylene (PP) mesh to reduce friction to wound tissues. Moreover, this double-network hydrogel exhibited a denser porous structure that controlled drug release without initial outburst. When testing the hydrogel-coated growth factor-loaded PP mesh on a rat model of OA, it was found that this composite material could reduce inflammation and promote granulation tissue growth. Therefore, our design provides a new strategy of material-assisted wound protection of OA and shows potential clinical applications.

1. Introduction

Abdominal sepsis, abdominal cavity syndrome (ACS), and abdominal wall defects caused by trauma or surgery are severe clinical problems.[1–3] There is a consensus on use of open abdomen (OA) therapy on patients with these diseases.[4] However, patients who receive OA will have a risk of developing intestinal fistula, which lowers the rate of definite fascia closure and gains the difficulties in abdominal wall reconstruction.[5]

Prosthetic materials are widely used in the technology of temporary abdominal closure (TAC) that provides protection to abdominal viscera during OA.[6,7] For example, polypropylene (PP) is a type of non-absorbable biocompatible synthetic material. PP mesh is chosen for TAC because of its excellent mechanical property that can provide enough strength to abdominal wall fascia and prevent abdominal retraction. However, clinical practice has revealed its shortcomings including the adhesion, erosion and fistula formation of exposed abdominal wound mainly due to the lack of soft tissues in coverage of visceral organs.[5]

Hydrogels are three-dimensional networks of polymeric materials that can absorb and retain large amounts of water or biological fluids.[8] Moreover, their internal porous structure mimics the extracellular matrix of native tissues to make them appropriate tissue scaffolds.[9] Therefore, hydrogels have shown great potentials in biomedical applications such as *in vivo* drug delivery and tissue engineering.[9–11] The stiffness is important for hydrogels to maintain its original shape, and the elasticity can enable the hydrogel to adapt to tissue movement and deformation.[12] However, these two characteristics seem to be contradictions for the same hydrogel, therefore interpenetrating double network hydrogels were proposed to obtain the stiff and elastic scaffolds.[13]

The polysaccharide, xanthan, has been widely used in the synthesis of hydrogels for tissue engineering,[14] wound healing[15,16] and other biomedical applications[17–19] due to its perfect biocompatibility. The molecular chain of xanthan is linear so that xanthan-based hydrogels tended to be stiffer, but less elastic. Poly(ethylene glycol) (PEG) is a type of water-soluble and biocompatible polymers.[14,20,21] Thiol-terminated poly(ethylene glycol) has been reported to form a hydrogel under UV light.[22] The resulting hydrogel has an outstanding elasticity but its stiffness is too low.

Considering the features of these two polymers, we reported an interpenetrating double network hydrogel through photopolymerization of glycidyl methacrylate-conjugated xanthan (XG) and 4-arm polyethylene glycol thiol (TPEG). The XG/TPEG hydrogel was gelated upon UV light exposure. We studied the micromorphology, swelling ratio, rheological properties and

[a]Department of Emergency Surgery, The Affiliated Hospital of Qingdao University, 16 Jiangsu Road, Qingdao 266000, P. R. China. E-mail: wpgzyz@163.com

[b]Lab for Trauma and Surgical Infections, Department of Surgery, Jinling Hospital, Affiliated to Southeast University, 305 East Zhongshan Road, Nanjing 210002, P. R. China. E-mail: 220163109@seu.edu.cn; Jiananr@gmail.com

† Electronic supplementary information (ESI) available. See DOI: 10.1039/c9ra10455k

controllable drug releasing ability of the hydrogel. Moreover, the PP mesh was coated by this hydrogel along with growth factors. The therapeutic effects of this composite material were evaluated on wounds of rats with OA.

2. Materials and methods

2.1 Materials

Xanthan gum (viscosity of 1% aqueous solution at 20 °C: 1450–2000 mPa s) was purchased from TCI Development Co. Ltd, Shanghai, China; glycidyl methacrylate (GMA) was purchased from Aladdin®, Shanghai, China; hydrochloric acid (36–38 wt%) was purchased from Jiuyi Reagent Co. Ltd, Shanghai, China; 4-arm PEG Thiol (TPEG, MW: $\sim 2 \times 10^4$) was purchased from Aladdin®, Shanghai, China; 2-hydroxy-4′-(2-hydroxyethoxy)-2-methylpropiophenone (I-2959) was purchased from Sigma-Aldrich®, St. Louis, MO, USA; recombinant human vascular endothelial growth factor 121 (rhVEGF121) was purchased from GenScript Co. Ltd, China; rhodamine B was purchased from Shanghai YSRIBIO Industrial Co. Ltd; PP mesh was purchased from B. Braun Medical International Trading Co. Ltd. All other reagents were of analytical reagent grade.

2.2 Fabrication of hydrogel networks

2.2.1 Synthesis of XG. A xanthan aqueous solution (0.6% w/v) was prepared by dissolving xanthan powders into deionized water, followed by stirring overnight. Then, 270 mL of such solution was poured into a round-bottom flask and heated to 80 °C using an oil bath (model: DF-101S, Xinbao Instrument Co. Ltd, Dongguan, China). Hydrochloric acid was used to adjust its pH to 4.2–4.8 and 1.88 mL of GMA was added dropwise into xanthan aqueous solution. After 12 h of stirring at 80 °C, the resultant solution was collected and then dialyzed for 3 days using dialysis membranes (molecular weight cut-off: 12–14 kDa) with deionized water being replaced every 8 h. Finally, the dialyzed solution was lyophilized in a freeze dryer (Xiongdi Instrument Co. Ltd, Zhengzhou, China).

2.2.2 Preparation of XG/TPEG hydrogel. XG was dissolved in phosphate buffer saline (PBS) containing 0.1% (w/v) I-2959 to obtain solution with the concentration of 10% (w/v). TPEG was dissolved in PBS containing 0.1% (w/v) I-2959 to obtain solution with the concentration of 8% (w/v). XG solution was mixed with TPEG solution at different volume ratios. The resulting solution was photoinitiated under UV-light exposure (365 nm, ~ 6.0 W cm^{-2}, model: UVPL-411, Yunhe Tech Co. Ltd, Suzhou, China)
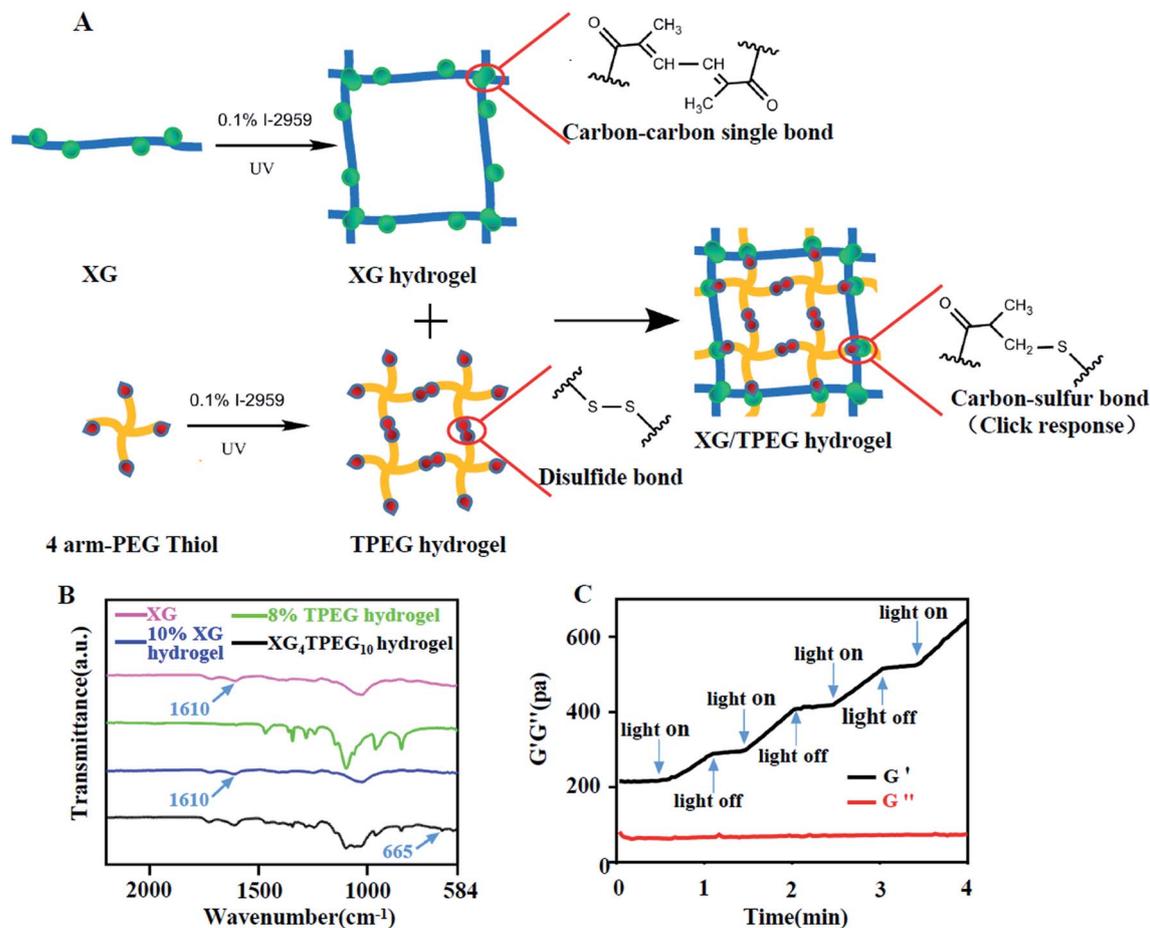

Fig. 1 Synthesis of XG/TPEG hydrogel. (A) Schematic diagram of the interpenetrating double-network XG/TPEG hydrogel. (B) Fourier transform infrared spectrum of XG hydrogel, TPEG hydrogel and XG/TPEG hydrogel. (C) The photosensitivity of XG/TPEG hydrogel revealed by the rheological test.

for 30 s. The exact reactions and volume ratios can be found in Fig. 1A, S1† and Table 1.

2.3 Characterization of materials

2.3.1 Fourier-transform infrared (FTIR) spectrometry. An FTIR spectrophotometer was applied to investigate the FTIR spectra of XG, TPEG and XG/TPEG hydrogels using a Nicolet-6700 spectrometer (Thermo®, USA) at room temperature in the wave number range of 4000–500 cm^{-1} by the potassium bromide disk technique. The powders of each polymer were ground to dry KBr disk, and 32 scans at a resolution of 4 cm^{-1} were used to record the spectra.

2.3.2 Morphology. A scanning electron microscope (model: S-4800, Hitachi®, Japan) was used to study the internal morphology of the hydrogel. Specifically, XG hydrogel, TPEG hydrogel and XG/TPEG hydrogel were freeze-dried. Then, these hydrogel samples were placed on a metal platform and their vertical sections were imaged after coating with a thin layer of gold.

2.3.3 Swelling ratio. The swelling ratio of XG hydrogel, TPEG hydrogel and XG/TPEG hydrogel was determined by the following formula:

$$\text{Swelling ratio} = (M_{\text{swollen gel}} - M_{\text{dried gel}})/M_{\text{dried gel}},$$

where $M_{\text{dried gel}}$ and $M_{\text{swollen gel}}$ stand for the mass of dried hydrogel and swollen hydrogel at equilibrium, respectively. Specifically, each hydrogel was firstly freeze-dried and then immersed in 5 mL of PBS at 37 °C. At each preset time, they were taken out and the surface moisture was wiped off using tissue paper. The hydrogels were weighed as soon as possible and then were returned to the original PBS.

2.4 Mechanical properties of the hydrogels

2.4.1 Rheological property. The rheological parameters were measured on a rheometer (model: MCR302, Anton Paar Co. Ltd, Austria) at 25 °C, whose gap of parallel plates was kept at 1 mm for this study. In the oscillatory frequency sweep experiment, the constant strain was fixed at 1%, and in the oscillatory time sweep experiment, the constant strain was fixed at 1% and frequency was fixed at 10 Hz. Four on-and-off cycles of UV light were applied on hydrogels with each cycle lasting for 30 s.

2.4.2 Compression testing. The hydrogel samples were prepared using a syringe to build a cylindrical shape with a diameter of 9 mm and length of 6 mm. A preload force of 0.1 N was set on the testing machine (model: BAB-10 MT, MTS Systems Co. Ltd, China). Each test was carried out at a compression velocity of 5 mm min^{-1}.

2.5 Water contact angles

Water contact angles of PP mesh, XG/TPEG hydrogel and XG/TPEG hydrogel-coated PP mesh were obtained by a JC2000D2 contact angle measuring system at ambient temperature. Static contact angles were recorded with a droplet volume of 2 μL. The static contact angles were measured at a neutral tilting angle (0°).

2.6 Injectability

This injectability of XG/TPEG hydrogel was also tested using the rheometer. The steady state shear flow was from 0.1 to 500 s^{-1} of shear rate. In addition, the practice of injection was performed using XG$_4$/TPEG$_{10}$ solution by handwriting the logo of Qingdao University, QDU. To make it clearer, the dye of methylene blue was added.

2.7 Cytocompatibility study

The cell biocompatibility was tested using a live/dead cell staining kit (Dalian MeiLun Biotech Co. Ltd.). 0.1 mL of 1.0×10^5 mL^{-1} L929 fibroblasts was seeded to the surface of XG$_4$/TPEG$_{10}$ hydrogel in a 24-well plate. Subsequently, 0.8 mL of DMEM medium was added to each well, and the samples were cultured for 24 h and 72 h. After cell staining, images were recorded using a fluorescence microscope. Moreover, we evaluated the cell proliferation by an extraction method. The XG/TPEG hydrogel was prepared in a 24-well plate following extraction using DMEM with 10% FBS for 24 h at 37 °C. Then, 0.1 mL of 1.0×10^5 mL^{-1} fibroblasts was incubated with the leachate (200 μL) for 24 h and 72 h. Subsequently, 10 μL of CCK-8 was added to each well, followed by incubation at 37 °C for another 4 h. After the solution was homogenized, the absorbance at 450 nm was measured. All experiments were performed in triplicate.

2.8 Drug controlled release

0.4 mL of XG solution (10% w/v) was mixed with 1.0 mL of 8% TPEG hydrazine solution along with rhodamine B (1 mg) or VEGF121 (5 μg) to obtain rhodamine B or rhVEGF121-loaded hydrogels. They were suspended in 10 mL PBS at 37 °C. 1 mL of PBS was collected at each preset timepoint and replaced with fresh PBS. The amount of rhodamine B was determined by a visible spectrophotometer at the absorbance of 554 nm and the amount of VEGF was determined using a VEGF ELISA assay kit (CUSABIO®, China). A standard calibration curve of absorption intensity *versus* concentration of VEGF was built as followed:

$$C = 6.7565 \times A - 0.368 \ (R^2 = 0.985),$$

where C represented the concentration of VEGF and A was the corresponding absorption intensity. The cumulative release was calculated from the ratio of actual VEGF content in the supernatant to the amount initially encapsulated in XG/TPEG hydrogel.

2.9 Open abdomen model

After being fasted overnight, twenty-four male Sprague-Dawley rats (180–250 g) were anesthetized through intraperitoneal injections of 10% chloral hydrate at 0.4 mL/100 g. Then, the hair

Table 1 Different volume ratios of XG and TPEG that were used to generate interpenetrating double network hydrogels

	XG$_4$TPEG$_5$	XG$_4$TPEG$_{10}$	XG$_3$TPEG$_{10}$	XG$_2$TPEG$_{10}$
10% XG	4	4	3	2
8% TPEG	5	10	10	10

of middle abdomen was clipped and the operative area was sterilized with iodophor for three times. A 2 × 3 cm partial abdominal defect was created by removing the full thickness of abdominal wall. Then, the rats were randomly divided into four groups: PP mesh control group, fibrin gel/PP mesh group, XG/TPEG hydrogel/PP mesh group and VEGF-load $XG_4/TPEG_{10}$ hydrogel-coated PP mesh group (Fig. S2†), with six rats in each group. PP meshes in each group were all sutured to the edge of the defects using 4/0 thread to prevent abdominal wall retraction. The rats were put back into cages and allowed free access to water and food. Seven days later, the rats were sacrificed and granulation tissues over the defects were harvested. Each granulation tissue was cut into three parts. Two parts were immersed in 10% neutral formaldehyde for further H&E staining, Masson trichrome staining and immunofluorescent staining, and the other part was for qPCR analysis (Table S1†) and western blot. All the animal care and experimental protocols were performed in strict accordance with the Chinese Guideline for the Care and Use of Laboratory Animals (Ministry of Science and Technology [2006] File No. 398) and approved by Animal Investigation Ethics Committee of the Affiliated Hospital of Qingdao University.

3. Results and discussion

3.1 Formation of XG/TPEG hydrogels

As shown in Fig. 1B, the spectrum of XG presents a characteristic peak at 1610 cm^{-1}, which refers to carbon–carbon double bonds

and suggests successful conjugation of GMA to xanthan. The intensity of this characteristic peak is reduced after photoinitiation of XG because of addition reaction that consumes carbon–carbon double bonds. The TPEG hydrogel has a similar spectrum to that reported previously.[23] In the XG/TPEG hydrogel, it not only shows a hybrid FTIR spectrum of XG hydrogel and TPEG hydrogel, but also newly presents an absorption peak of carbon–sulfur bonds at 665 cm^{-1}. This indicates that XG hydrogel and TPEG hydrogel can interact with each other by click response during the interpenetrating process. Moreover, the stiffness of XG/TPEG hydrogel is increased upon UV exposure (Fig. 1C), which implies that this hydrogel is photosensitive.

3.2 Morphology

The morphology of XG hydrogel, TPEG hydrogel and XG/TPEG hydrogel is shown in Fig. 2A. These hydrogels have three-dimensional porous structure with varied pore sizes. Moreover, it can be observed that in XG/TPEG hydrogel, TPEG fragments are spread over the pores of XG hydrogel, which can support the architecture of XG hydrogel. This is the exact reason that explains why the addition of TPEG can increase the elasticity of XG hydrogel.[24]

3.3 Swelling ratio

Swelling ratio is an important parameter that not only evaluates hydrogel's absorbing ability of tissue exudates, but also
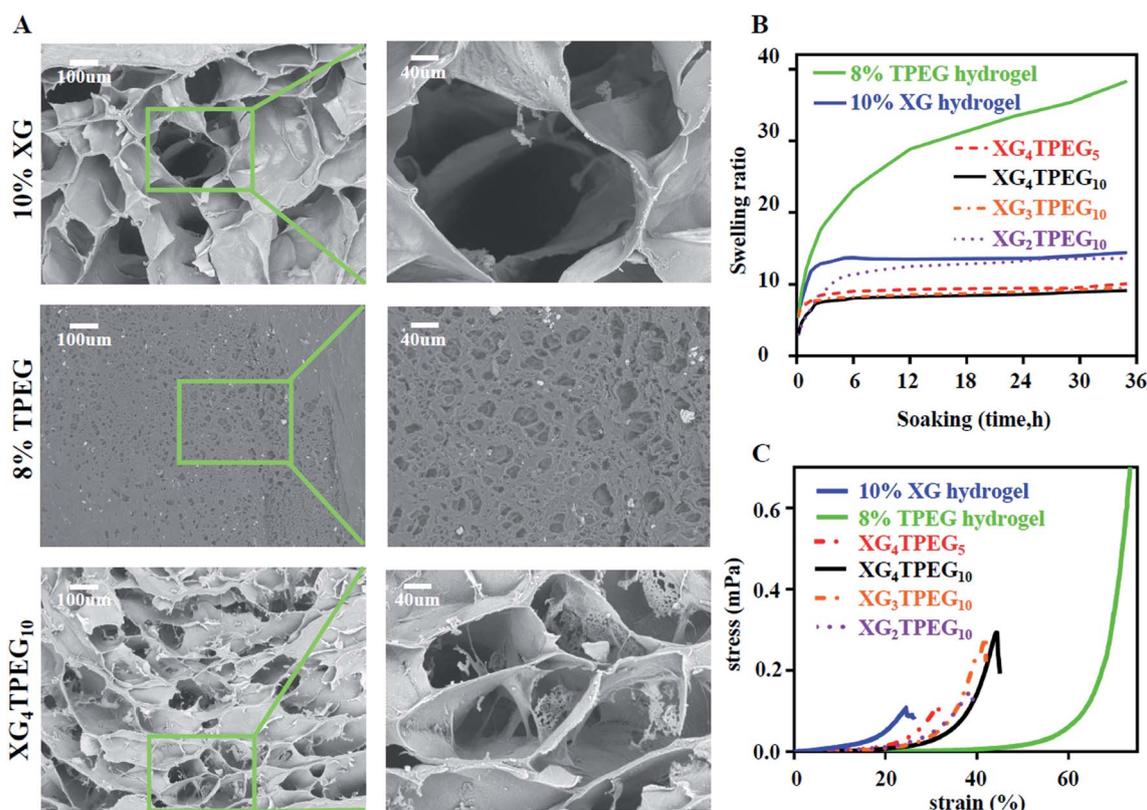

Fig. 2 Physical properties of XG/TPEG hydrogel. (A) SEM images of XG hydrogel, TPEG hydrogel and XG/TPEG hydrogel after lyophilization. (B) Swelling ratios of XG hydrogel, TPEG hydrogel and XG/TPEG hydrogels. (C) Stress–strain diagrams of XG hydrogel, TPEG hydrogel and XG/TPEG hydrogels.
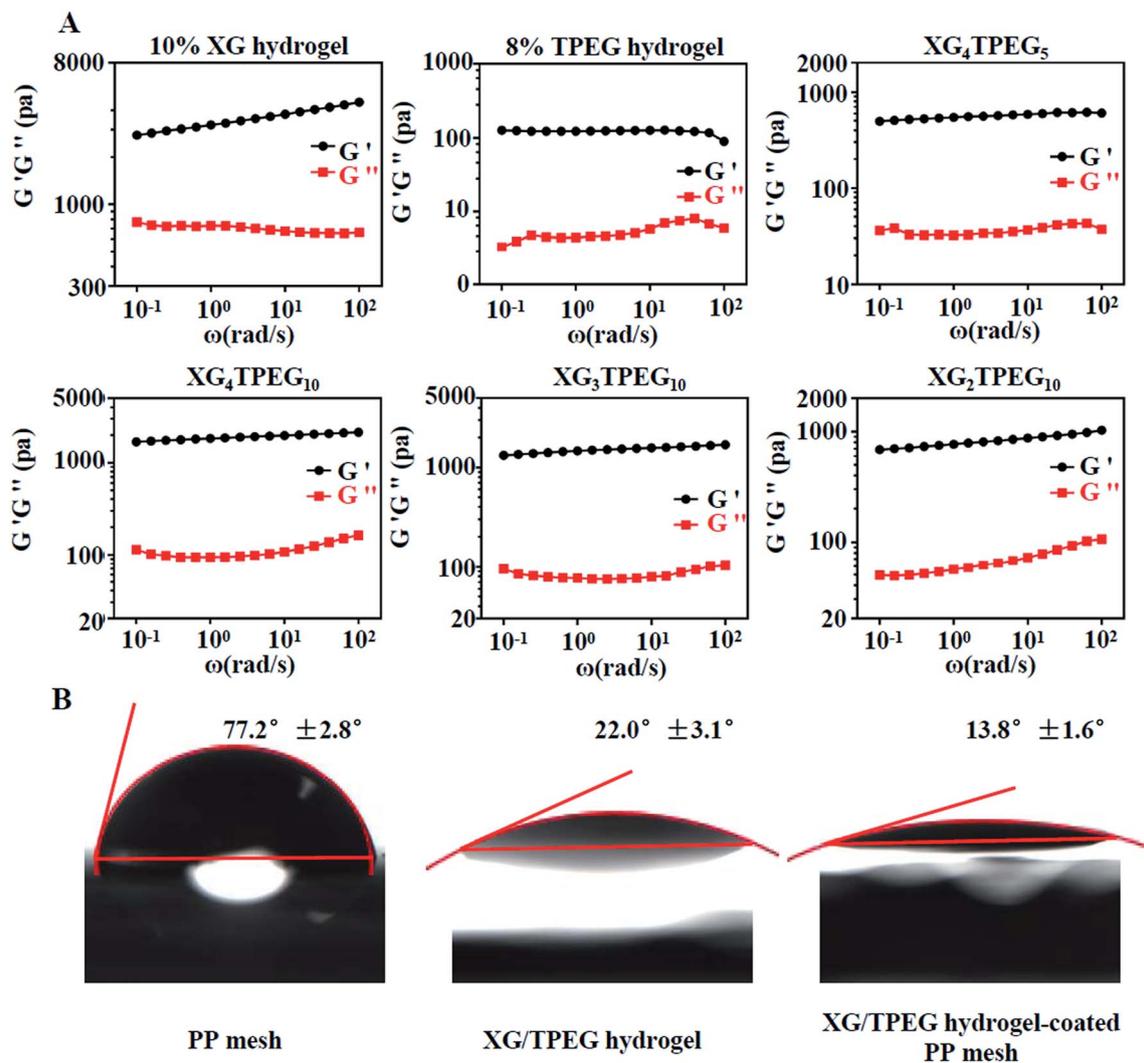
Fig. 3 Rheological tests and hydrophilia of XG/TPEG hydrogels. (A) Frequency-dependent oscillatory shear rheology of XG hydrogel, TPEG hydrogel and XG/TPEG hydrogels. (B) Water contact angles of PP mesh XG/TPEG hydrogel and XG/TPEG hydrogel-coated PP mesh.

its volume stability in wet conditions. In this study, we find that XG/TPEG hydrogels have lower swelling ratios compared with XG hydrogel or TPEG hydrogel alone (Fig. 2B). It implies

that the XG/TPEG hydrogel has a more stable volume that reduces the pressure on covered viscera when applied *in vivo*. It can effectively prevent the risk of high intraabdominal
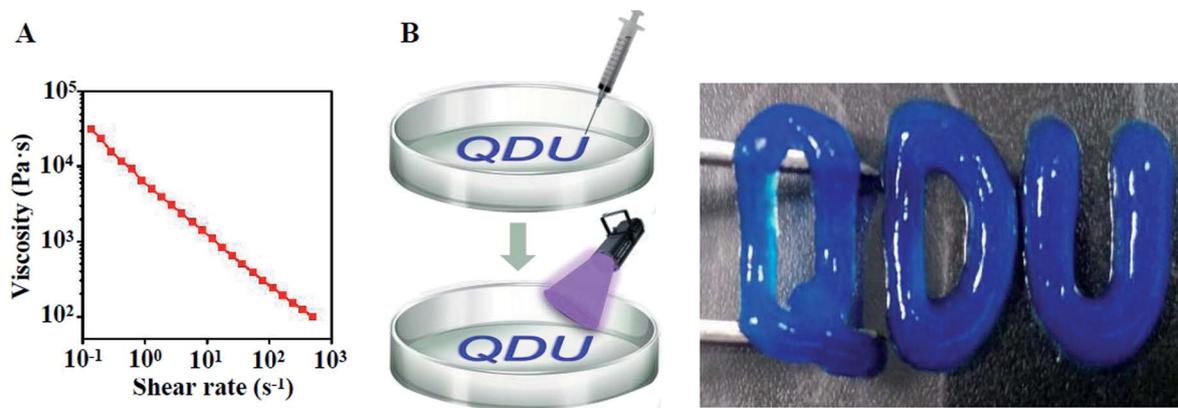
Fig. 4 Injectability of XG/TPEG hydrogel. (A) Shear-thinning property of XG/TPEG mixed solution. (B) Handwriting of Qingdao University logo by injection and photopolymerization of XG/TPEG hydrogel.
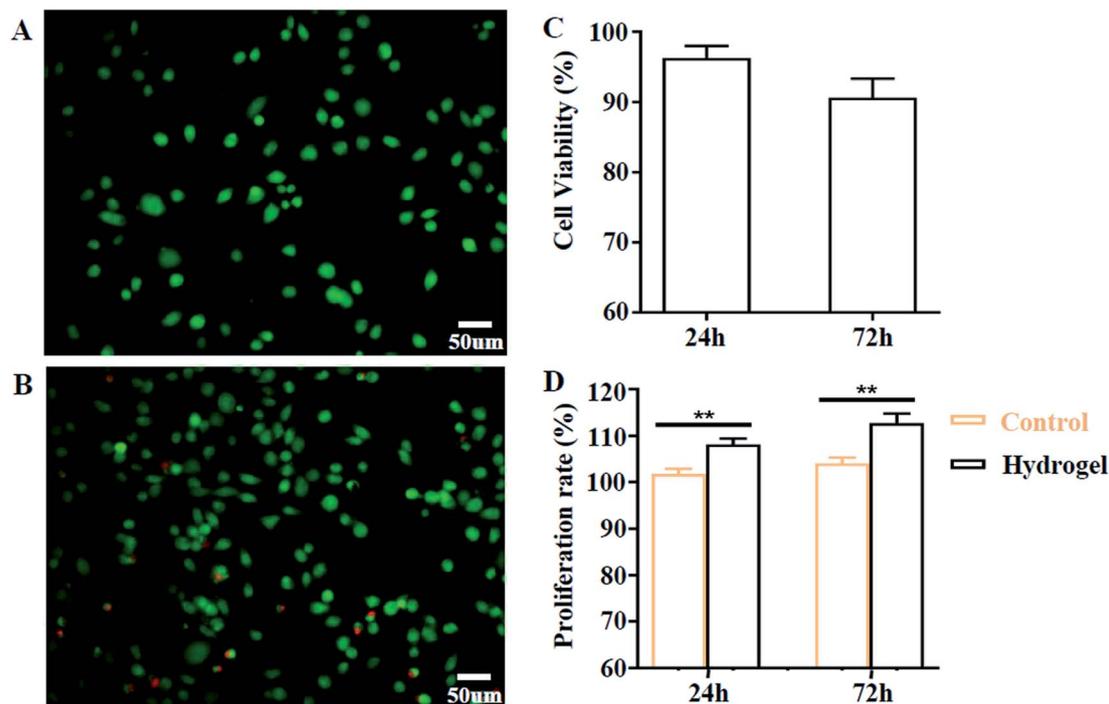
Fig. 5 *In vitro* cytocompatibility of XG/TPEG hydrogel. (A–C) Live/dead staining after co-culture of fibroblasts on the surface of XG/TPEG hydrogel. (A) 24 h; (B) 72 h; (C) cell viability. (D) Cell proliferation rate of fibroblasts when cultured in BMDM medium and leachate for 24 h and 72 h. **, $P < 0.01$.

pressure, which otherwise leads to hypoperfusion of abdominal organs.

3.4 Mechanical strength

Then, we examined that whether the strategy of interpenetrating double network made the hydrogel stiff and elastic. As shown in Fig. 2C and 3A, 10% XG hydrogel shows the highest storage modulus (G') of 4 kPa at 0.1 rad s^{-1} but the lowest compressive strain of 24%, while 8% TPEG hydrogel shows the lowest G' of 0.11 kPa at 0.1 rad s^{-1} but the highest compressive strain of over 80%.[25] When combining these two hydrogels, it is observed that XG/TPEG hydrogel achieves a balance of stiffness and elasticity. By screening, the XG$_4$/TPEG$_{10}$ hydrogel has been chosen for later PP mesh coating because its stiffness and elasticity are the most optimized among all hydrogel combinations, which facilitate to get a steady hydrogel coating with tolerance to external shear force.

3.5 Water contact angles

Water contact angles reflect hydrophilicity of materials. The angle over 90° implies hydrophobic materials and the angle less than 90° means hydrophilic materials. From the results of water contact angle testing in Fig. 3B, we conclude that the PP mesh is a hydrophilic material, but its hydrophilia is inadequate.
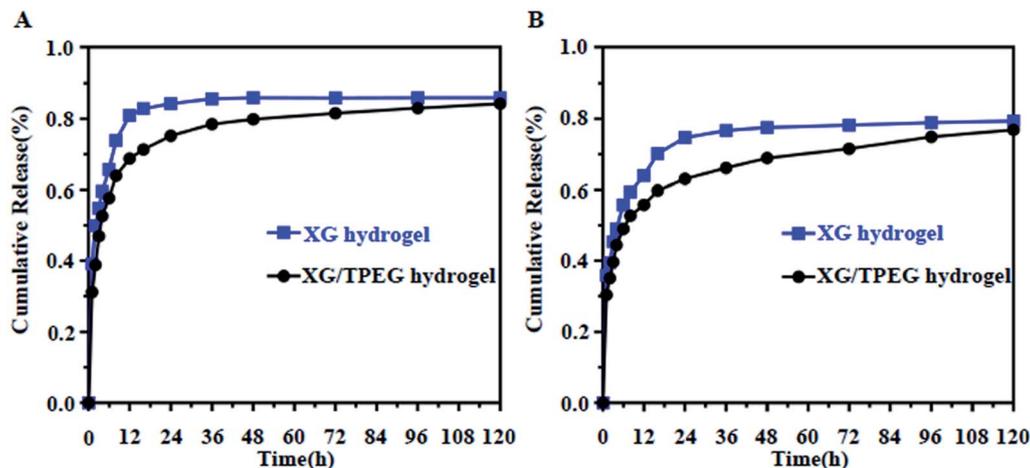

Fig. 6 *In vitro* drug releasing profile by simple XG hydrogel and XG/TPEG hydrogel carriers. (A) Rhodamine B profile. (B) VEGF profile.

Differently, $XG_4/TPEG_{10}$ hydrogel has an excellent hydrophilia, which can improve the hydrophilicity of PP mesh by coating. By this way, the composite PP mesh will provide an appropriate scaffold that supports cell adhesion and growth, thus the repair of defected abdominal wall can be accelerated.

3.6 Injectability

The injectability of $XG_4/TPEG_{10}$ mixed solution is attributed to its shear thinning property shown in Fig. 4A, which was tested using a rheometer. Moreover, we exhibited its injectability by

handwriting of Qingdao University logo. After photocuring, this logo could be lifted up (Fig. 4B). This injectable ability enables that the XG/TPEG mixed solution can fill up any irregular shape of coated materials.[26]

3.7 Cytocompatibility study

Biocompatibility is a prerequisite factor for biomaterials to have practical applications. Here, we evaluated this aspect by cell co-culture with $XG_4/TPEG_{10}$ hydrogel and its leachate. As indicated in Fig. 5A–C, the fibroblast viability is more than 90% after 24 h
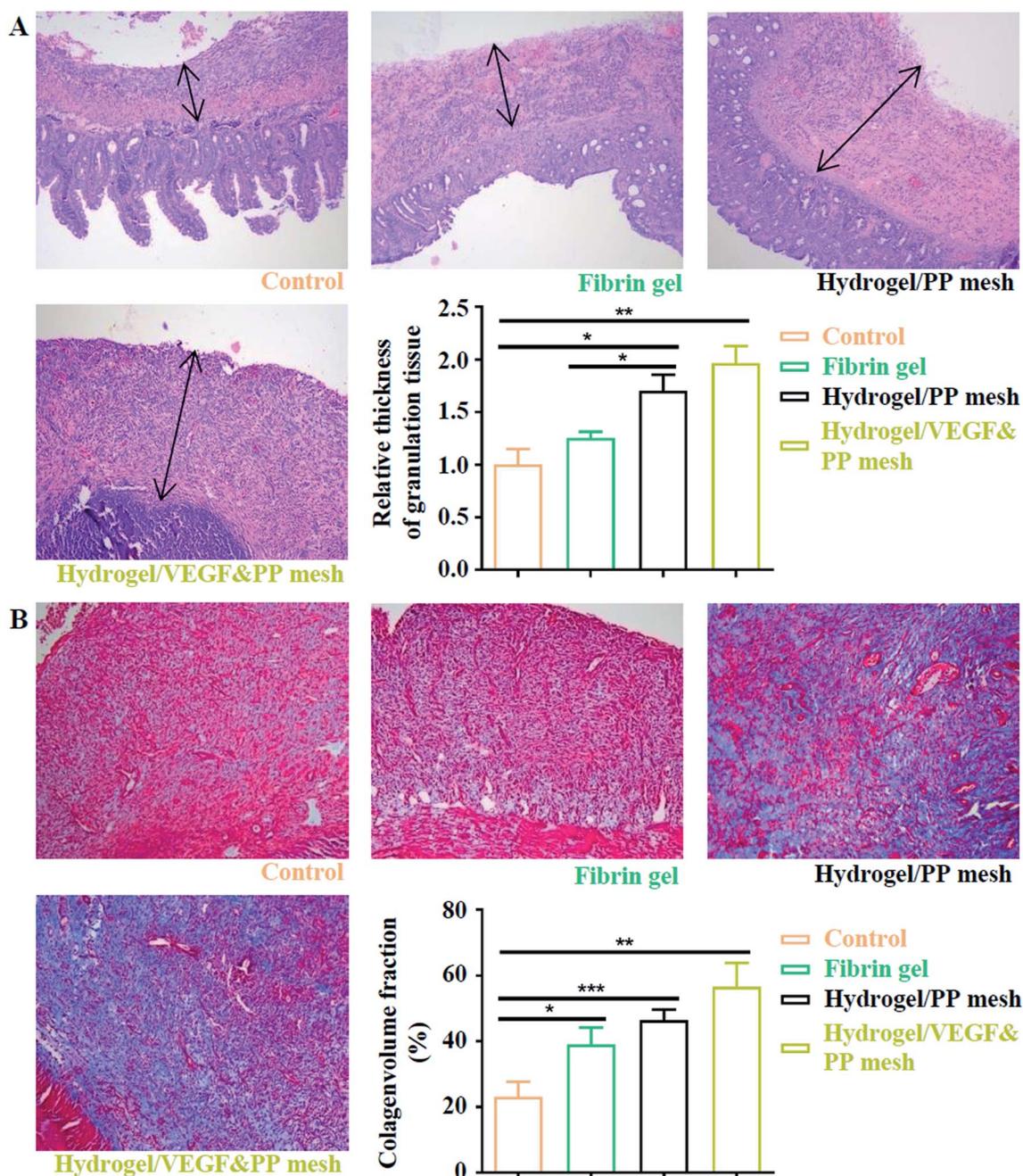

Fig. 7 Assessment of four potential treatments on protection of abdominal wall defect of rat models. (A) HE staining of regenerative abdominal wall tissues (blank arrows: regenerative tissues), 10×. *$P < 0.05$, **$P < 0.01$. (B) Masson staining of regenerative abdominal wall tissues, 10×. *$P < 0.05$, **$P < 0.01$, ***$P < 0.001$.

and more than 85% after 72 h, which suggests that this hydrogel hasn't acute cytotoxicity to fibroblasts. Moreover, the leachate of $XG_4/TPEG_{10}$ hydrogel is found to promote the cell proliferation of fibroblasts (Fig. 5D). It is because the degraded polysaccharide derivative (XG) in the leachate may behavior as a stimulant to up-regulate the cell growth and migration.[14] Above results demonstrate the safety of $XG_4/TPEG_{10}$ hydrogel coating of PP mesh for wounds of OA.

3.8 Drug controlled release

Hydrogel has been reported as an effective carrier to improve the wound healing by adding bioactive drugs such as tissue growth factor-β (TGF-β), fibroblast growth factor (FGF) and VEGF, because the drugs can regulate specific cellular signaling in a long term.[23,27–29] As previously mentioned, the micromorphology of XG hydrogel is changed after interpenetrating with TPEG hydrogel, therefore it is necessary to investigate the variation of drug release patterns by using a representative small-

molecule drug, *i.e.*, rhodamine B and a large-molecule drug, *i.e.*, VEGF. It was found that it was more obvious for these two drugs released more slowly in $XG_4/TPEG_{10}$ hydrogel than these in simple XG hydrogel (Fig. 6A and B). The potential reason is the smaller and interlaced micropores that can restrict the release of loaded drugs. This experiment points to the advantage of this interpenetrating double network hydrogel in cytokine therapy of tissue engineering.

3.9 Open abdomen model

Finally, we evaluated the $XG_4/TPEG_{10}$ hydrogel-coated pp mesh on wounds of OA rat models. It is indicated in Fig. 7A and B that $XG_4/TPEG_{10}$ hydrogel-coated pp mesh could improve the regeneration of granulation tissues and collagen deposition for OA wounds compared with control group and fibrin gel group possibly because of XG bioactivities. After loading with VEGF, the therapeutic efficacy could be further enhanced owing to the synergistic biological effects of XG and VEGF. This was
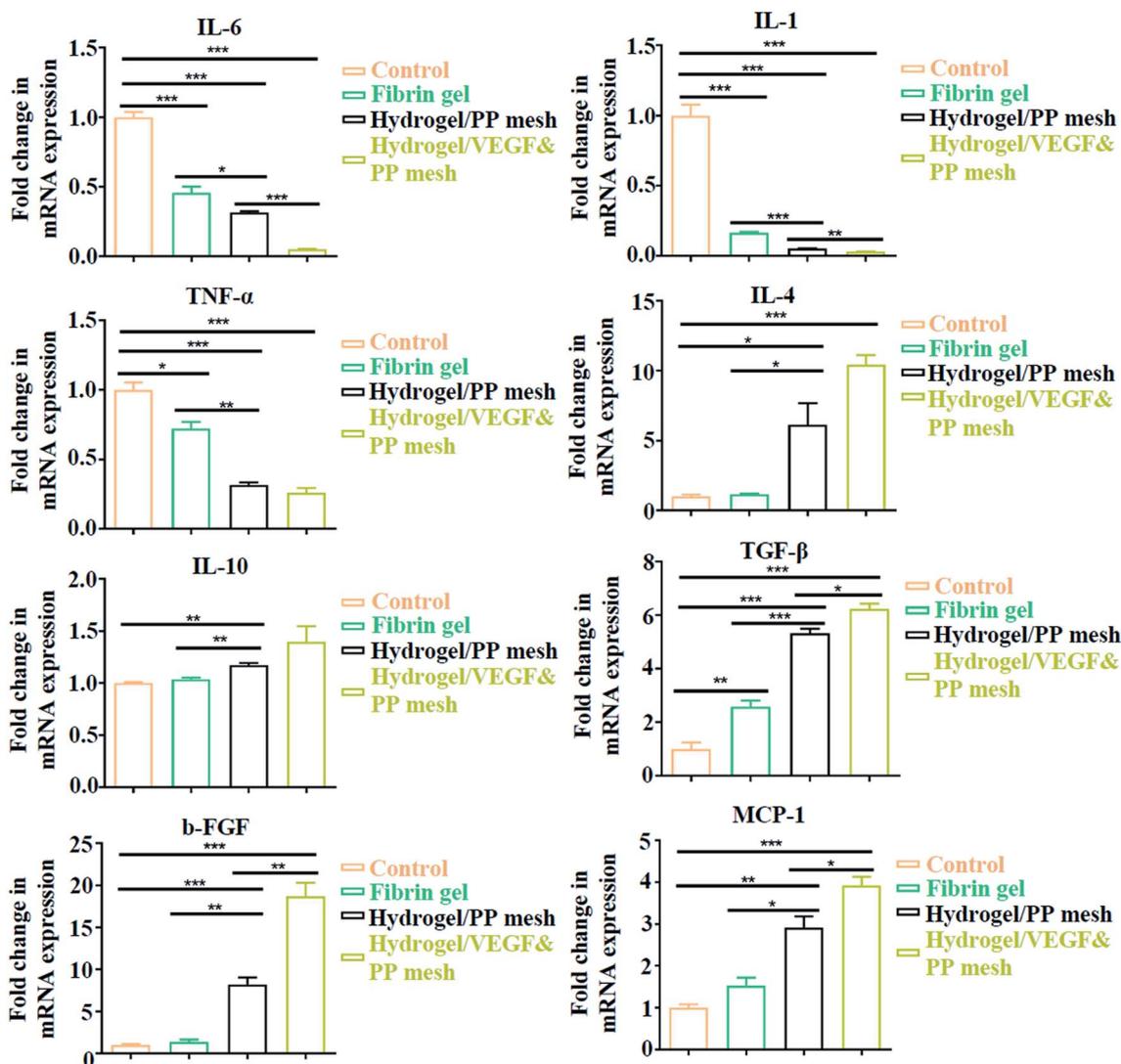

Fig. 8 Quantitative analysis of gene expressions in four groups, expressed as fold change. *P < 0.05, **P < 0.01, ***P < 0.001.

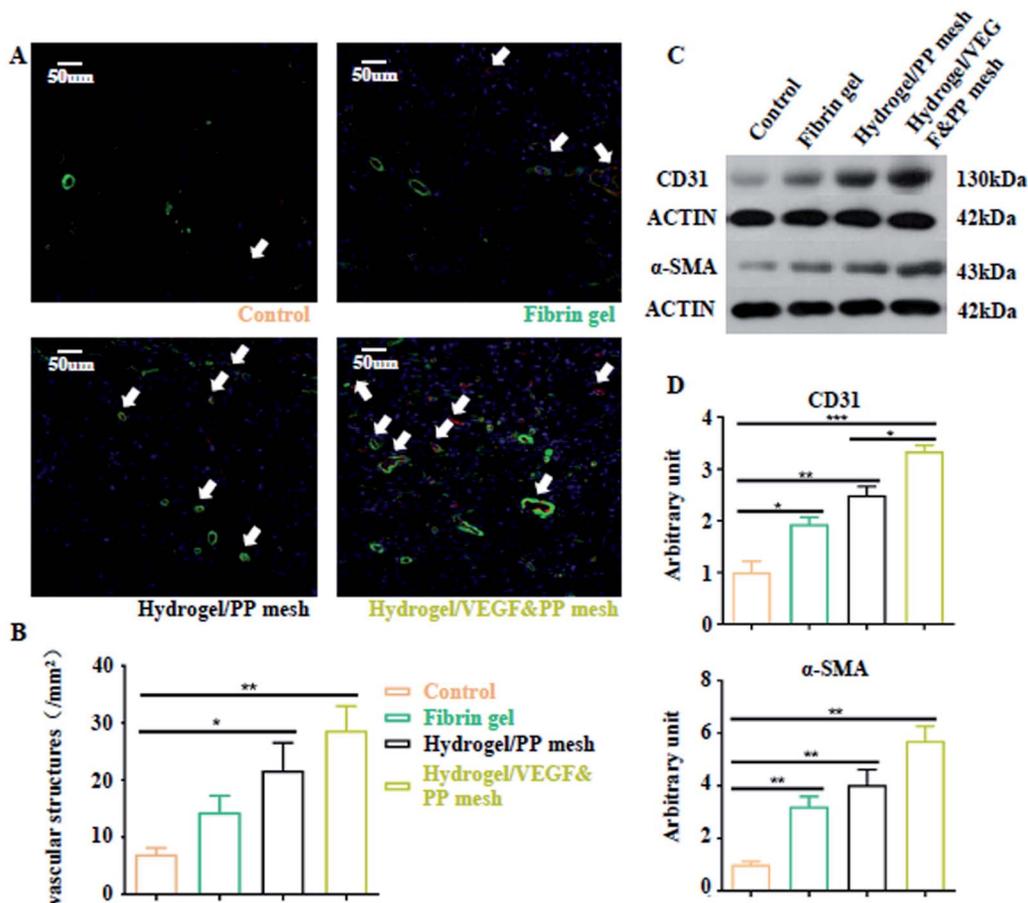**Fig. 9** Neovascularization of four groups. (A) Double fluorescence staining of vessels by CD31 and α-SMA in four groups. (B) Quantification of vessel density in granulation tissues in four groups. *$P < 0.05$, **$P < 0.01$. (C) Western blotting images of CD31 and α-SMA expressions in granulation tissues of four groups. (D) Analysis of gray intensity of CD31 and α-SMA in the corresponding western blotting tests. *$P < 0.05$, **$P < 0.01$, ***$P < 0.001$.

consistent with the findings of molecular transductions within granulation tissues (Fig. 8). Pro-inflammatory signaling was significantly reduced in XG_4/$TPEG_{10}$ hydrogel-coated pp mesh group and VEGF-loaded hydrogel-coated group such as interleukin (IL)-6, IL-1 and tumor necrosis factor (TNF)-α, while their anti-inflammatory signaling was increased such as IL-4 and IL-10. Moreover, angiogenesis signaling such as TGF-β and FGF, and cellular chemotaxis signaling such as monocyte chemoattractant protein (MCP)-1 were also significantly up-regulated. Apart from the genetic expression level, the angiogenic effects were also confirmed at protein expression level. As shown in Fig. 9A, B and C, D, the density and biomarkers of vessels such as CD31 and α-SMA were increased correspondingly. To our interest, the whole molecular signaling maps in the regenerated tissues are in line with the M2 polarization of macrophages characterized by low pro-inflammatory signaling and high tissue healing signaling, which is an important cellular phenotypic transformation during tissue repair.[30] The rapid process of granulation tissue regeneration has significant clinical meanings that can prevent intestinal fistula formation on the OA wounds and make a good preparation for skin grafting.

4. Conclusions

In this study, we synthesized a new interpenetrating double-network XG/TPEG hydrogel with optimal stiffness and elasticity. This hydrogel is well hydrophilic and biocompatible to fibroblasts for their growth and attachment. Moreover, by the formation of dense and interlaced micropores, growth factors can have a slower releasing rate when carried by this interpenetrating double-network hydrogel in comparison to individual XG hydrogel. When we coated XG/TPEG hydrogel on PP mesh, this composite material showed great protective functions on OA wounds by promoting rapid granulation tissue formation, especially in combination of growth factor therapy. All in all, our study provides an advantageous TAC biomaterial with good mechanical strength, drug releasing ability and wound healing for management of defected abdominal wall, and will have great potential clinical applications.

Author contributions

Peige Wang, Jianan Ren and Jinjian Huang conceived and designed the experiments; Ze Li, Changliang Wu, Zhen Liu,

Conflicts of interest

The authors declared no potential conflicts of interest with respect to the research, authorship, and/or publication of this article.

Acknowledgements

References

1 F. Caviggioli, F. M. Klinger, A. Lisa, L. Maione, D. Forcellini, V. Vinci, L. Codolini and M. Klinger, *J. Case Rep. Med.*, 2014, **2014**, 235930.

2 G. L. Carlson, H. Patrick, A. I. Amin, G. McPherson, G. MacLennan, E. Afolabi, G. Mowatt and B. Campbell, *Ann. Surg.*, 2013, **257**, 1154–1159.

3 J. A. Carr, *J. Am. Coll. Surg.*, 2013, **216**, 135–146.

4 G. Popivanov, K. Kjossev and V. Mutafchiyski, *Il G. Chir.*, 2017, **38**, 267–272.

5 F. Coccolini, D. Roberts, L. Ansaloni, R. Ivatury, E. Gamberini, Y. Kluger, E. E. Moore, R. Coimbra, A. W. Kirkpatrick, B. M. Pereira, G. Montori, M. Ceresoli, F. M. Abu-Zidan, M. Sartelli, G. Velmahos, G. P. Fraga, A. Leppaniemi, M. Tolonen, J. Galante, T. Razek, R. Maier, M. Bala, B. Sakakushev, V. Khokha, M. Malbrain, V. Agnoletti, A. Peitzman, Z. Demetrashvili, M. Sugrue, S. Di Saverio, I. Martzi, K. Soreide, W. Biffl, P. Ferrada, N. Parry, P. Montravers, R. M. Melotti, F. Salvetti, T. M. Valetti, T. Scalea, O. Chiara, S. Cimbanassi, J. L. Kashuk, M. Larrea, J. A. M. Hernandez, H. F. Lin, M. Chirica, C. Arvieux, C. Bing, T. Horer, B. De Simone, P. Masiakos, V. Reva, N. DeAngelis, K. Kike, Z. J. Balogh, P. Fugazzola, M. Tomasoni, R. Latifi, N. Naidoo, D. Weber, L. Handolin, K. Inaba, A. Hecker, Y. Kuo-Ching, C. A. Ordonez, S. Rizoli, C. A. Gomes, M. De Moya, I. Wani, A. C. Mefire, K. Boffard, L. Napolitano and F. Catena, *World J. Emerg. Surg.*, 2018, **13**, 7.

6 Q. Huang, J. Li and W. Y. Lau, *Gastroent. Res. Pract.*, 2016, **2016**, 2073260.

7 Y. Deng, J. Ren, G. Chen, G. Li, X. Wu, G. Wang, G. Gu and J. Li, *Sci. Rep.*, 2017, **7**, 2699.

8 V. H. Phan, T. Thambi, H. T. Duong and D. S. Lee, *Sci. Rep.*, 2016, **6**, 29978.

9 C. Ghobril and M. W. Grinstaff, *Chem. Soc. Rev.*, 2015, **44**, 1820–1835.

10 S. J. Buwalda, K. W. Boere, P. J. Dijkstra, J. Feijen, T. Vermonden and W. E. Hennink, *J. Controlled Release*, 2014, **190**, 254–273.

11 S. Park, S. Mun and Y. R. Kim, *Food Res. Int.*, 2018, **105**, 440–445.

12 J. Huang, Z. Li, Q. Hu, G. Chen, Y. Ren, X. Wu and J. Ren, *iScience*, 2018, **8**, 40–48.

13 C. Curme, T. Preis, H. E. Stanley and H. S. Moat, *Proc. Natl. Acad. Sci. U. S. A.*, 2013, **111**, 11600–11605.

14 A. Kumar, K. M. Rao and S. S. Han, *Carbohydr. Polym.*, 2018, **180**, 128–144.

15 A. I. Raafat, N. M. El-Sawy, N. A. Badawy, E. A. Mousa and A. M. Mohamed, *Int. J. Biol. Macromol.*, 2018, **118**, 1892–1902.

16 T. Phaechamud, P. Issarayungyuen and W. Pichayakorn, *Int. J. Biol. Macromol.*, 2016, **85**, 634–644.

17 M. Kang, O. Oderinde, S. Liu, Q. Huang, W. Ma, F. Yao and G. Fu, *Carbohydr. Polym.*, 2019, **203**, 139–147.

18 E. A. Elizalde-Pena, I. A. Quintero-Ortega, D. G. Zarate-Trivino, A. Nuno-Licona, J. Gough, I. C. Sanchez, D. I. Medina and G. Luna-Barcenas, *Mater. Sci. Eng., C*, 2017, **78**, 892–900.

19 S. M. Kuo, S. J. Chang, H. Y. Wang, S. C. Tang and S. W. Yang, *Carbohydr. Polym.*, 2014, **114**, 230–237.

20 W. L. Murphy, T. C. McDevitt and A. J. Engler, *Nat. Mater.*, 2014, **13**, 547–557.

21 H. Y. Liu, H. D. Nguyen and C. C. Lin, *Adv. Healthcare Mater.*, 2018, **7**, e1800954.

22 C. Zhang, Q. Dong, K. Liang, D. Zhou, H. Yang, X. Liu, W. Xu, Y. Zhou and P. Xiao, *Int. J. Biol. Macromol.*, 2018, **119**, 270–277.

23 F. Lv, L. Mao and T. Liu, *Mater. Sci. Eng., C*, 2014, **43**, 221–230.

24 S. Li, J. Yi, X. Yu, H. Shi, J. Zhu and L. Wang, *ACS Biomater. Sci. Eng.*, 2018, **4**, 872–883.

25 L. J. Macdougall, V. X. Truong and A. P. Dove, *ACS Macro Lett.*, 2017, **6**, 93–97.

26 Q. Wei, S. Jiang, R. Zhu, X. Wang, S. Wang and Q. Wang, *iScience*, 2019, **14**, 27–35.

27 H. Madry, A. Rey-Rico, J. K. Venkatesan, B. Johnstone and M. Cucchiarini, *Tissue Eng., Part B*, 2014, **20**, 106–125.

28 A. Sivashanmugam, P. Charoenlarp, S. Deepthi, A. Rajendran, S. V. Nair, S. Iseki and R. Jayakumar, *ACS Appl. Mater. Interfaces*, 2017, **9**, 42639–42652.

29 J. Huang, Y. Deng, J. Ren, G. Chen, G. Wang, F. Wang and X. Wu, *Carbohydr. Polym.*, 2018, **186**, 54–63.

30 A. R. Reeves, K. L. Spiller, D. O. Freytes, G. Vunjak-Novakovic and D. L. Kaplan, *Biomaterials*, 2015, **73**, 272–283.